



UNIVERSITY OF LEEDS

This is a repository copy of *Probing the charging mechanisms of carbon nanomaterial polyelectrolytes*.

White Rose Research Online URL for this paper:

<http://eprints.whiterose.ac.uk/99485/>

Version: Accepted Version

Article:

Hodge, SA, Tay, HH, Anthony, DB et al. (6 more authors) (2014) Probing the charging mechanisms of carbon nanomaterial polyelectrolytes. *Faraday Discussions*, 172. pp. 311-325. ISSN 1359-6640

<https://doi.org/10.1039/c4fd00043a>

Reuse

Unless indicated otherwise, fulltext items are protected by copyright with all rights reserved. The copyright exception in section 29 of the Copyright, Designs and Patents Act 1988 allows the making of a single copy solely for the purpose of non-commercial research or private study within the limits of fair dealing. The publisher or other rights-holder may allow further reproduction and re-use of this version - refer to the White Rose Research Online record for this item. Where records identify the publisher as the copyright holder, users can verify any specific terms of use on the publisher's website.

Takedown

If you consider content in White Rose Research Online to be in breach of UK law, please notify us by emailing eprints@whiterose.ac.uk including the URL of the record and the reason for the withdrawal request.

PAPER

Probing the charging mechanisms of carbon nanomaterial polyelectrolytes

Cite this: DOI: 10.1039/x0xx00000x

Stephen A. Hodge,^a Hui Huang Tay,^a David B. Anthony,^a Robert Menzel,^a David J. Buckley,^b Patrick L. Cullen,^b Neal T. Skipper,^b Christopher A. Howard,^b and Milo S. P. Shaffer^{a*}

Received 00th January 2012,
Accepted 00th January 2012

DOI: 10.1039/x0xx00000x

www.rsc.org/

Chemical charging of single-walled carbon nanotubes (SWCNTs) and graphenes to generate soluble salts shows great promise as a processing route for electronic applications, but raises fundamental questions. The reduction potentials of highly-charged nanocarbon polyelectrolyte ions were investigated by considering their chemical reactivity towards metal salts/complexes in forming metal nanoparticles. The redox activity, degree of functionalisation and charge utilisation were quantified via the relative metal nanoparticle content, established using thermogravimetric analysis (TGA), inductively coupled plasma atomic emission spectroscopy (ICP-AES) and X-ray photoelectron spectroscopy (XPS). The fundamental relationship between the intrinsic nanocarbon electronic density of states and Coulombic effects during charging is highlighted as an important area for future research.

Introduction

Carbon nanomaterials, including both single-walled carbon nanotubes (SWCNTs) and graphene have impressive intrinsic mechanical, thermal and (opto)electronic properties.¹ Applications of these materials have been slow to emerge due to challenging synthesis and post-synthesis processing requirements. The desire for stable suspensions/solutions of monodispersed species to enable liquid-phase processing has led to the development of numerous aqueous-surfactant² and non-aqueous³ dispersion procedures. Unfortunately, most routes rely on high-power ultrasonication to exfoliate and disperse the nanomaterials, which tends to degrade the desirable properties, for example via shortening and the introduction of structural defects.⁴ Subsequently, lengthy ultracentrifugation steps are typically required to remove non-exfoliated material, leading to limited overall process yields and scalability.

An attractive approach to dissolve carbon nanomaterials without damaging their structure is via charging protocols, as outlined in Fig. 1. Fullerene (C_{60}), SWCNT and graphene polyelectrolyte anions, known as fulleride, nanotubide and

graphenide species, respectively, can be generated following reduction using alkali metal/liquid NH_3 ,⁵⁻⁸ alkali metal naphthalide/tetrahydrofuran (THF),^{9, 10} or electrochemically in non-aqueous electrolytes.¹¹ In addition, electrochemical oxidation was recently demonstrated to generate nanotube cations, known as nanotubium species.¹² All reductive charging techniques insert electrons into the carbon π^* orbitals, shifting the Fermi energy of the nanocarbon density of states (DOS), resulting in increased reactivity. Subsequent reaction may take place via redox or electrophilic addition reactions that may involve a single-electron transfer (SET) (i.e. radical based reactions).¹³⁻¹⁸

The degree of functionalisation (d.o.f.), typically reported as a ratio of functional addends to carbon atoms on the nanocarbon species, is a quantitative measure of the reaction yield. However, reactivity depends strongly on the amount of charge per carbon atom,¹⁹ its potential or chemical activity, the nature of the reactant added, and the reaction mechanism(s).

PAPER

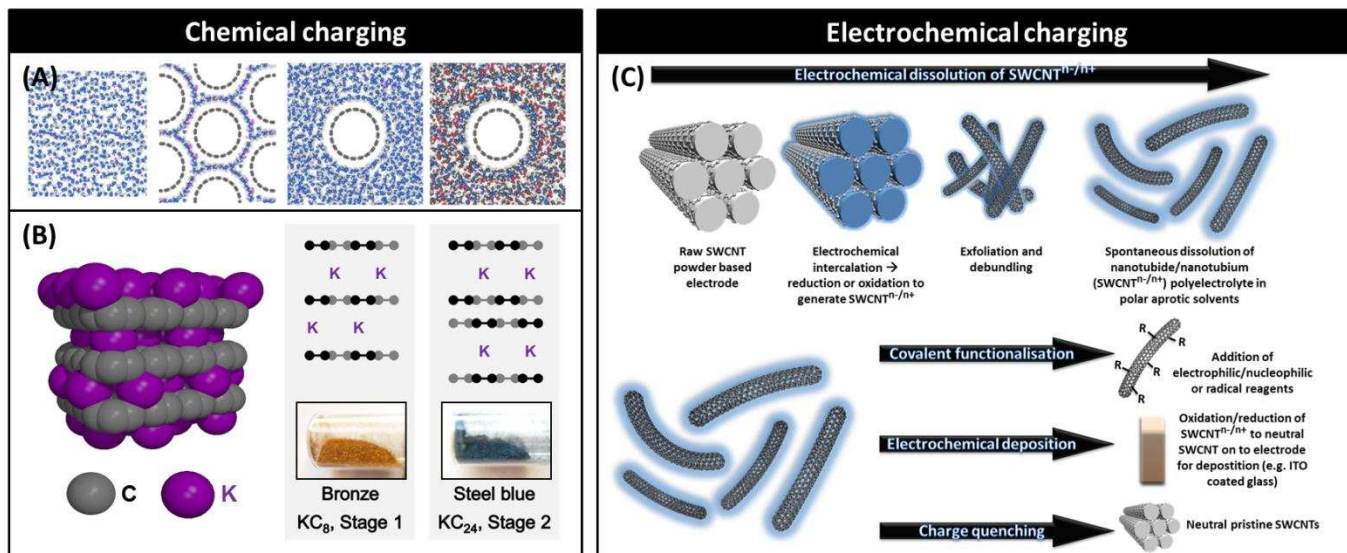


Fig. 1 Selected examples of charged carbon nanomaterials. (A) Nanotubide anions generated using alkali metal/liquid ammonia. Reproduced with permission from ref. 5. (B) Graphite intercalation compounds (GICs) generated by the vapour transport method²⁰ using potassium. (C) Electrochemical processing to generate nanotubide anions and nanotubium¹² cations. Modified with permission from ref 11. The charged materials shown in (A) and (B) are used in the current investigation.

It follows that to enhance the d.o.f., the charge per carbon atom should be increased, and a reactant with a more favourable reduction or SET potential added. The degree of nanocarbon exfoliation is also a crucial factor in enhancing the d.o.f.; in fact steric constraints can even be significant, for fully exfoliated SWCNTs/graphenes in which all atoms in principle lie on the ‘surface’.¹⁶ Ultimately, controlling the d.o.f. is critical: for example, too many functional addends can cause the loss of (opto)electronic and mechanical properties, too few and there may be no benefit to nanocarbon solubility or compatibility with a polymer matrix.²¹ The first nanotube redox potentials have been probed using spectroelectrochemical methods,²²⁻²⁴ and the redox potentials of reactants in aqueous systems are well studied. However, the exact potential of charged nanocarbon polyelectrolytes and redox potentials of reactants in anhydrous, aprotic solvents are not well known.

The DOS of nanocarbon species are known to be complex but continuous, leading to the observation of bulk-continuum voltammetry.^{11, 12} The DOS for their ions has not yet been determined and is likely to vary with charge density. In this discussion paper, the potential/chemical activity of nanotube and graphene polyelectrolyte anions will be used to reduce a range of metal salts to generate zero oxidation state metal atoms/nanoparticles (NPs) on the carbon surface, as a route to probe the unclear relationship between added charge density and potential.

It has been observed that nanotubes/graphene act as reducing agents towards metal salts; even neutral SWCNTs can spontaneously reduce Au³⁺ and Pt²⁺ salt solutions to form their respective M⁰_(metal) NPs on the nanotube surface.²⁵ Nanotubides and graphenides can significantly increase the yield of this metal deposition due to the higher reducing potential of the carbon.^{26, 27} In principle, the use of metal salts should proceed by simple redox chemistry, avoiding electrophilic addition and radical reactive pathways. The initial hypothesis was that, for nanocarbon polyelectrolyte anion reactions with metal salts, the resulting metal to carbon (M:C) atomic ratio (i.e. the d.o.f.) should be defined by the initial charge transfer and the metal reduction potential. Based on the quantified d.o.f., the reduction potential of the nanocarbon polyelectrolyte should be predicted by integrating the areas of reacted electrons (charge utilisation yield) and unavailable charge (between the metal reduction potential and the undoped nanocarbon Fermi level) on the nanotube/graphene DOS plot, shown by the schematic diagram in Fig. 2.

Results and discussion

Sodium nanotubide experiments

Preliminary experiments used raw HiPco SWCNTs, reduced using solutions of sodium metal in liquid ammonia to give a NaC₁₀ SWCNT salt following evaporation of the ammonia (note that a small amount of ammonia remains coordinated to

the metal). This salt was left to spontaneously dissolve into anhydrous N,N-dimethylformamide (DMF) as in previous methodology.⁵ The resulting dissolved SWCNT fraction used for reaction had a concentration of 0.6 mg/mL (80% yield of dissolution).

Two metal chloride salts (MnCl_2 and ZnCl_2), typically used as precursors to generate the respective $\text{M}^0_{(\text{metal})}$ NPs using a wide range of reducing agents,^{28, 29} were added to the nanotubide dispersions in a three times excess to sodium. For these NPs, exposure to the atmosphere following reaction is likely to cause partial oxidation of the NPs. Following oxidative thermogravimetric analysis (TGA) of the washed, filtered and dried nanotube/metal samples, metal oxide residues remain (Electronic Supplementary Information (ESI) Fig. S1). Raw HiPco contains ~30 wt% iron oxide originating from the catalyst used in its synthesis. Reaction with MnCl_2 showed only a subtle increase in metal oxide content from the raw material, however, the ZnCl_2 reaction yielded a ~7 wt% increase. Scanning electron microscopy (SEM) images of metal halide treated SWCNTs before TGA revealed NPs containing manganese and zinc, confirmed using energy-dispersive X-ray spectroscopy (EDX) (Fig. 3). These relative reactivities were expected, in-line with the reduction potentials of their respective metal salts (standard reduction potentials: $\text{Zn}^{2+} + 2\text{e}^- \rightarrow \text{Zn}^0$, -0.76 V, and $\text{Mn}^{2+} + 2\text{e}^- \rightarrow \text{Mn}^0$, -1.18 V vs. SHE (standard hydrogen electrode)).

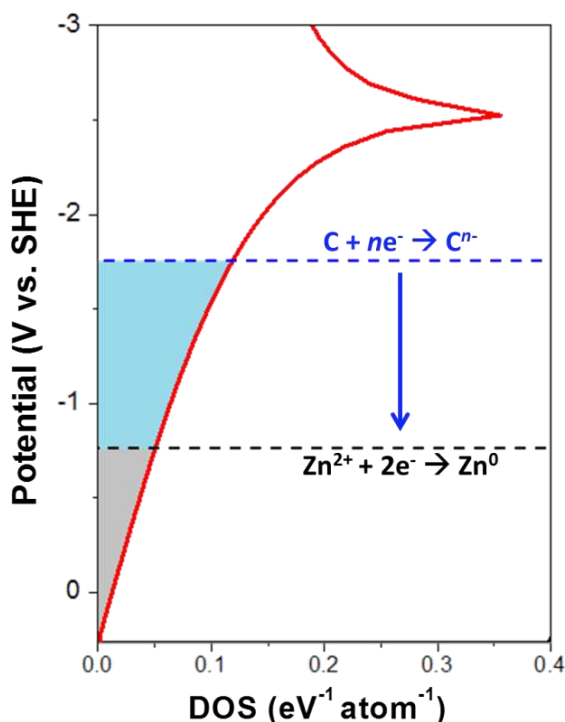


Fig. 2 DOS of a graphene crystal based on the tight-binding approximation (data values from ref. 30), neglecting Coulombic effects. The position of the graphene Fermi level (E_F) was previously determined⁹ as +0.022 V vs. saturated calomel electrode (SCE) (~+0.263 V vs. SHE). The dashed black line represents the standard reduction potential for Zn^{2+} (-0.76 V vs. SHE), the dashed blue line represents a possible position of the nanocarbon reduction potential. Available electrons for reaction with Zn^{2+} are shaded blue, whereas the unavailable

electrons are shaded grey. As the available charge is used, the potential of the nanocarbon will shift towards the Zn^{2+} reduction potential until the reaction reaches completion.

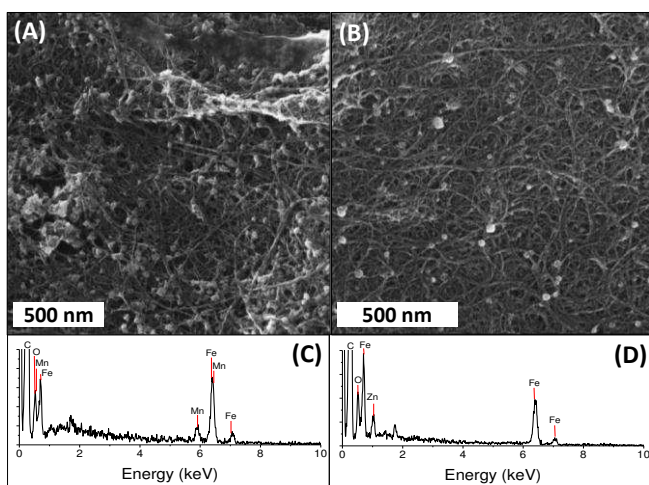


Fig. 3 SEM images of the metal NPs generated from reaction of NaC_{10} nanotubide with (A) MnCl_2 and (B) ZnCl_2 , respectively. (C) and (D) are the complementary EDX spectra for Mn and Zn NPs, respectively.

Having successfully generated NPs for the manganese and zinc systems, the ability to extend this electrochemical series to a whole set of metal NPs exists. However, due to the presence of the (oxidised) iron catalyst, the possibility of competitive reduction reactions cannot be avoided. Due to the unknown charge per carbon atom in the dissolved fraction compared to the undissolved material, and the complex density of states (including mixtures of metallic and semi-conducting species with different band gaps and Fermi level positions) presented by nanotube samples, it is complex to confirm the exact reduction potential of the NaC_{10} SWCNT salt. Instead, a simpler charged carbon nanomaterial was studied. Graphite intercalation compounds (GICs) that can be exfoliated to monolayer graphenide species,⁶ produced from Madagascan natural flake graphite are an ideal model system as they are have large crystallite size, high purity and an absence metal contaminants.

Potassium graphenide experiments

GICs have been studied for many years.³¹ The stage 1 compound, KC_8 , as shown in Fig. 1 (B), has been used directly as a strong reducing agent in many organic reactions.^{32, 33} KC_8 is more reducing than naphthalene³⁴ generating the naphthalene radical anion in THF (-2.24 V vs. SHE), and has been exploited to prepare active metals including Zn, Sn, Ti, Fe, Pd and Ni (from reaction with the metal halides) highly dispersed on the graphite surface.³² These metal-graphites demonstrated high catalytic activity for a wide range of synthetically useful reactions. A suggested mechanism for KC_8 reactivity was proposed by Ebert.³⁵ In this model, two potassium species, K^0 and K^+ , exist between the graphite layers in order to account for the incomplete charge transfer to the graphite. In this way, KC_8 was proposed to exhibit a "hybrid" chemistry, in which

electrons still "associated" with K⁰ might react differently from those transferred to graphite. Thus, potassium species at edge sites react with a reduction potential close to that of metallic potassium (-2.93 V vs. SHE). As this metallic potassium is used up, the relative reduction potential of the resultant KC_{8-n} compound lowers. In the case of solubilised potassium graphenide, the charge transfer and consequent reduction potential of the KC₈ will be altered by solvation effects including the stabilisation of graphenide sheets and the degree of potassium ion dissociation.

Further insight can be gained from recent measurements of the electronic structure of bulk potassium GICs.³⁶ In crystals of KC₈ and KC₂₄, the Fermi energy relative to that of pure graphite is shifted as the electrons occupy the graphitic π* band. The Fermi level shift has been measured using photoemission spectroscopy³⁶ to be -1.35 eV in KC₈ and ~-0.75 eV in KC₂₄. It is important to note that, in these unexfoliated materials, there is only partial charge transfer (~44%) from the potassium atoms to the π* bands, with the rest thought to reside in an electronic band associated with the intercalant superlattice.³⁷

In the experiments presented here, the potassium ions of solvated graphenide become dissociated from the charged graphene sheets to some extent (with some degree of counterion condensation³⁸), presumably leading to an increase in charge transfer from the potassium to the graphene π* band. The Fermi level shift in the limit of complete charge transfer from the potassium to the graphene can be approximated³⁹ using the relationship, $E_F = -\sqrt{n\pi} \cdot \hbar v_F$, where $\hbar v_F = 5.52 \text{ eV}\text{\AA}$ and n is the number of electrons per graphene unit cell area (5.24 \AA^2) (KC_{8,n} = 0.0477, KC_{24,n} = 0.0158). Thus, Fermi level shifts of -2.14 eV (-1.88 V vs. SHE) and -1.23 eV (-0.997 V vs. SHE) are calculated for KC₈ and KC₂₄, respectively. Testing a range of metal salts with a range of reduction potentials should allow a comparative experimental reduction potential to be deduced. Ideally, the reactivities of KC₈ and KC₂₄ should fall within these Fermi energy shifts for partial and complete charge transfer.

Potassium GICs were produced via the vapour transport method,²⁰ to give the corresponding characteristic bronze stage 1 KC₈ and steel blue stage 2 KC₂₄ compounds (Fig. 1B). Graphenide dispersions were produced in dry N-methylpyrrolidone (NMP). Controlling the reaction stoichiometry as a route to produce smaller NPs, or even covalently bound metal atoms to the graphenides was investigated. Reactions were performed using the exact stoichiometry as number of charges available for reduction, e.g. for M²⁺ salts, M²⁺:K = 0.5:1, M⁺ salts, M⁺:K = 1:1, etc., with results shown in Table 1 and ESI Table S1. Elemental analysis of the TGA residues with inductively coupled plasma atomic emission spectroscopy (ICP-AES) was used to accurately discriminate between the alkali metal oxide content and the generated metallic NPs. Since ICP-AES has limits of detection on the order of parts per billion (ppb), the combination of these techniques allows the unequivocal quantification of the carbon to metal atomic ratio.

As with the case of NaC₁₀ nanotubide reduction, there is still a higher reactivity for highly charged graphenides (KC₈) towards zinc compared to manganese. KC₂₄, however, does not have sufficient reducing power to react with the manganese (II) salt.

Table 1. Reactivity of KC₈ and KC₂₄ graphenide polyelectrolytes with metal salts/complexes.

Metal cation (M ⁿ⁺)	Reduction potential (V vs. SHE)	KC ₈ (M:C atomic ratio)	Charge utilisation yield ^{c,d} (%)	KC ₂₄ (M:C atomic ratio)	Charge utilisation yield ^{c,d} (%)
Mn ²⁺ (MnCl ₂)	-2.01 ^a , -1.18 ^b	446	3.6	No reaction	-
Zn ²⁺ (ZnCl ₂)	-1.13 ^a , -0.76 ^b	107	15.0	489	9.8
Cu ²⁺ (CuCl ₂)	-0.34 ^b	887	1.8	-	-
Cu ⁺ (CuMes)	+0.44 ^a , +0.52 ^b	10	78.5	-	-

^a derivation from cyclic voltammetry experiments in 0.1 M KClO₄/NMP,

^b standard reduction potential. ^c TGA and ICP measurements. ^d refer to Fig. 2 for charge utilisation yield definition. – not measured.

Copper salts, with a reduction potential similar to that of uncharged graphene, would be expected to reveal the highest reactivity. In fact, a very low reactivity was observed for KC₈ with CuCl₂; this failure could be due to the one electron reduction of CuCl₂ to the intermediate CuCl.⁴⁰

To enhance the reactivity, highly soluble mesityl copper(I) (CuMes) was used in order to avoid the two-step reduction.⁴¹ The solution turned red/brown, indicating the formation of Cu⁰_(metal) in solution; subsequent UV-vis absorption spectroscopy (ESI Fig. S2) revealed the surface plasmon absorption (~570 nm) typical for metallic CuNPs.⁴² The resultant Cu NPs generated by KC₂₄ were surprisingly air stable for approximately 1 week. Since the CuNPs were free in solution and not bound to the graphene, filtration of the reaction mixture in air would have resulted in the oxidation of unreacted CuMes to Cu⁰_(metal). Therefore, KC₈ generated Cu NPs were precipitated with toluene and air-free centrifugation was performed to sediment the graphene/Cu NPs. The supernatant containing unreacted CuMes was removed and the graphene/Cu NPs were filtered and washed for subsequent characterisation. It was not possible to precipitate the KC₂₄ generated NPs for reaction quantification. Since the reduction potential for Cu⁺ lies below the Fermi level for undoped graphene,⁹ a 100% charge utilisation yield would be expected. However, only a 78.5% yield was observed by TGA and ICP-AES, probably due to the extensive processing steps involved in extracting the KC₈-Cu NP sample.

The metal halide to potassium stoichiometry was also investigated for the KC₈-ZnCl₂ reaction, including a three times excess of ZnCl₂ as used for the previous nanotubide experiments (Table 2). SEM (Fig. 4) revealed nanoparticles formed at all stoichiometries, and the overall d.o.f. slightly increased with increased ZnCl₂ concentration. X-ray photoelectron spectroscopy (XPS) (ESI Fig. S3) showed the

typical Zn 2p_{3/2} binding energy peak position in zinc oxide,⁴³ ZnO (~1022 eV). Due to the comparatively larger size of the NPs formed at excess zinc concentrations, the surface sensitive XPS measurements are likely to underestimate the true Zn:C atomic ratio. Combined TGA and ICP measurements probe the full bulk of the samples and, therefore, provide a more reliable determination of the d.o.f.

Table 2. Comparison between KC₈-ZnCl₂ reactivity with varying Zn²⁺:K stoichiometry

Stoichiometry Zn ²⁺ :K	KC ₈ (Zn:C atomic ratio) TGA/ICP	KC ₈ (Zn:C atomic ratio) XPS
0.5:1	107	161
3:1	92	205
10:1	88	259

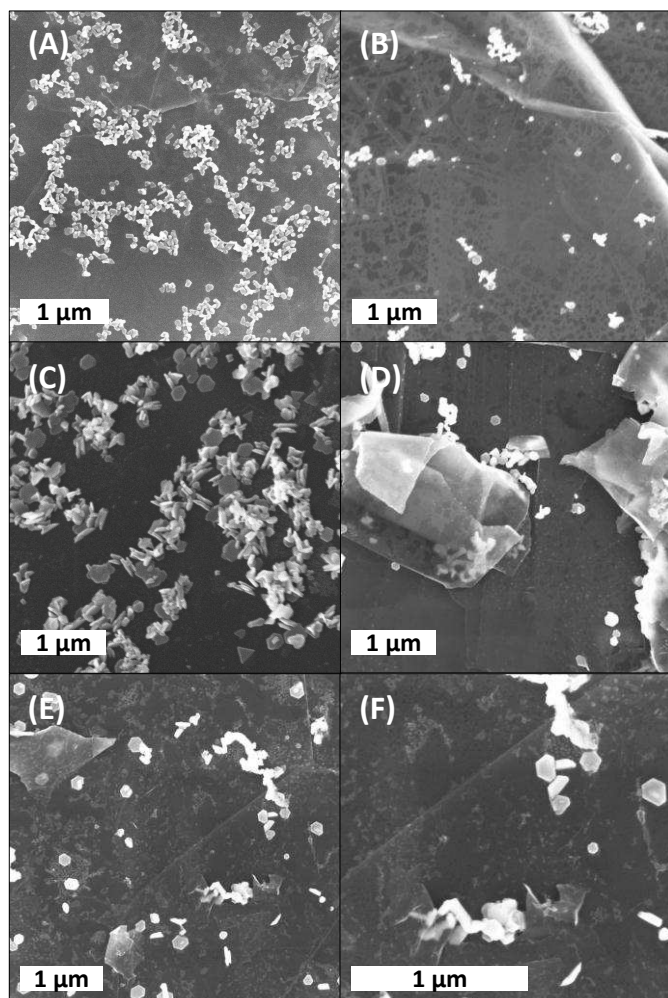


Fig. 4 SEM images of the generated ZnNPs from reaction of KC₈ with ZnCl₂ at varying stoichiometry. Two different regions are shown for each case, (A),(B) Zn²⁺:K 0.5:1; (C),(D) Zn²⁺:K 3:1; (E),(F) Zn²⁺:K 10:1.

Deriving the reduction potentials of KC₈ and KC₂₄

In the present case, reactions were performed using 10⁻³ M concentrations in non-aqueous solutions. Consequently, the reduction potentials of the metal salts/complexes are likely to

be significantly different to standard reduction potentials that are based on 1 M solute concentrations, 25°C. The reduction potential of the metal salt/complex is shifted dependent on its concentration as defined by the Nernst equation, $E_{M^{n+}/M} = E^0_{M^{n+}/M} + ((RT/nF) \ln [M^{n+}])$, where E⁰ is the standard reduction potential, and n is the number of electrons involved. It will be important to adjust the reduction potentials accordingly, in order to determine the extent of reaction.

For M²⁺ reactions (M²⁺:K = 0.5:1): KC₈ (2.6 mM M²⁺), E = E⁰ + (-0.076 V), KC₂₄ (0.87 mM M²⁺), E = E⁰ + (-0.091 V). For M⁺ reactions (M⁺:K = 1:1): KC₈ (5.2 mM M⁺), E = E⁰ + (-0.135 V), KC₂₄ (1.74 mM M⁺), E = E⁰ + (-0.163 V). A higher concentration of Zn²⁺ ions promotes a more favourable reduction to zinc (at Zn²⁺:K 3:1, 15.6 mM, E = E⁰ + (-0.053 V)), and Zn²⁺:K 10:1, 52 mM, E = E⁰ + (-0.038 V)), leading to the observed higher degree of functionalisation, Zn:C (by TGA/ICP-AES), and relatively larger nanoparticle formation, refer to Table 2 and Fig. 4.

The reduction potentials for MnCl₂, ZnCl₂ and CuMes at typical reaction concentrations were deduced from cyclic voltammetry experiments in 0.1 M KClO₄/NMP electrolyte (Fig. 5). The Ag/AgNO₃ non-aqueous reference electrode was calibrated against ferrocene/ferrocenium (Fc/Fc⁺) (+0.08 V vs. Ag/AgNO₃) and then adjusted to the SHE (Fc/Fc⁺ = +0.64 V vs. SHE). The derivation of metal salt/complex reduction potentials from their cyclic voltammetric behaviour is discussed in ESI Fig. S4. The experimentally determined metal reduction potentials vs. SHE used for deriving the KC₈ and KC₂₄ reduction potentials are: MnCl₂ (-2.01 V), ZnCl₂ (-1.13 V), CuMes (+0.44 V). Fig. 6 shows a schematic view of all the above reduction potentials with respect to the graphene DOS. As described in Fig. 2, integrating the DOS between the reduction potential of the metal salt and the zero density Fermi level of undoped graphene affords an area of unavailable electron density for reaction. Integration of the respective "charge utilisation yield" (Table 1) above the metal salt potential provides an estimate of the KC_x reduction potential. The KC₂₄ reduction potential could only be derived from its reactivity with ZnCl₂; integration of the DOS to 9.8% charge utilisation above the Zn potential gives -1.21 V vs. SHE symbolised by the blue coloured band in Fig. 5B.

For KC₈, the MnCl₂ reaction (3.6% charge utilisation) affords a reduction potential of -2.04 V vs. SHE, however, KC₈ reactivity with ZnCl₂ (15% charge utilisation) suggests a reduction potential of -1.25 V vs. SHE. Even at a 20-fold increase of Zn²⁺:K stoichiometry (10:1), the reduction potential is relatively unchanged (-1.27 V vs. SHE). The reaction of KC₈ with CuMes suggests a reduction potential of -1.70 V, falling within the same region. This range of potentials are symbolised by the bronze coloured band in Fig. 5B. Based on the observed reactivity with MnCl₂, it would be reasonable to suggest that the KC₈ potential should lie towards the upper region of this band. The derived reduction potentials closely resemble the band corresponding to literature potentials discussed above (Fig. 5A). The significant difference between the KC₈ reduction potentials derived from the manganese and zinc reactivity

might be due to various factors; most importantly, the DOS presented here is for a perfect graphene system and may not

accurately represent the true DOS of highly doped graphene in solution.

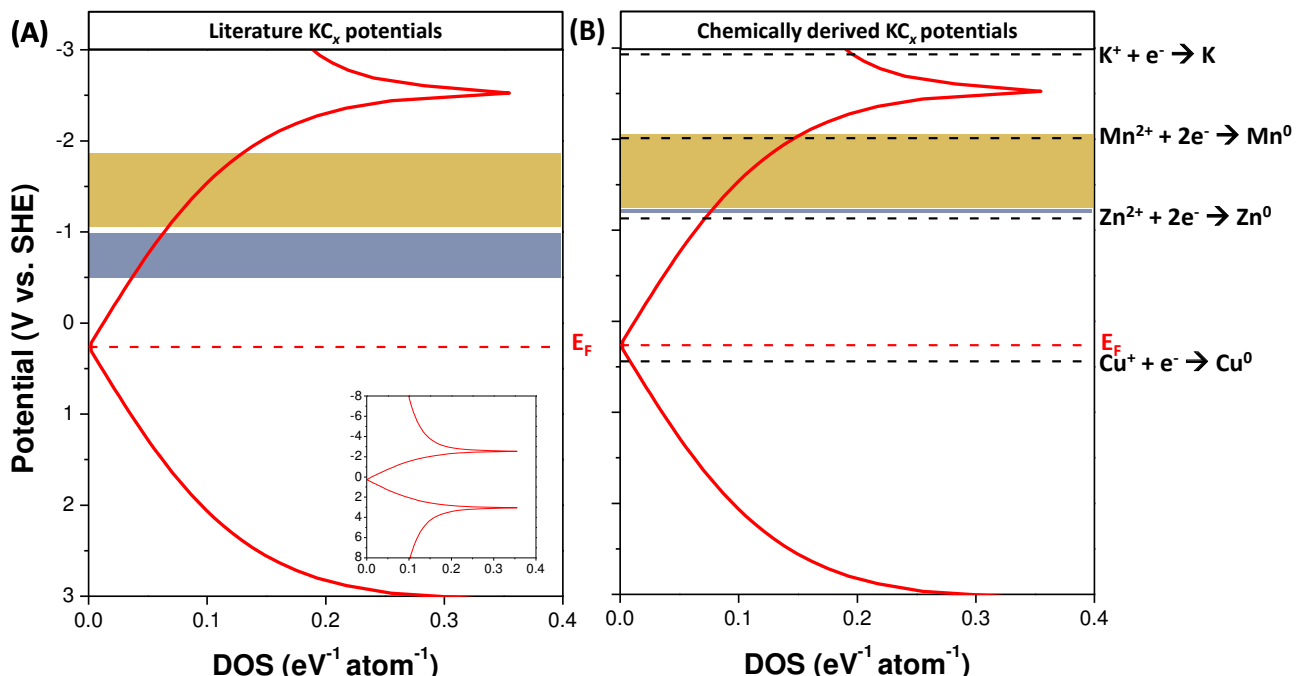


Fig. 5 DOS of a graphene crystal based on the tight-binding approximation (data values from ref. 30). Black dashed lines represent the reduction potentials for the metal compounds derived in this study in 0.1 M $KClO_4$ /NMP. In (A), the bronze and blue shaded bands represent the approximate levels of doping for KC_8 and KC_{24} , respectively, based on experimental data for bulk GIC crystals³⁶ (partial charge transfer) and approximations³⁹ for complete charge transfer. Inset shows the perfect graphene DOS over a wider potential range. In (B), the bronze band represents the derived reduction potentials for KC_8 and KC_{24} , respectively, based on charge utilisation yields in reactions with $MnCl_2$, $ZnCl_2$ and $CuMes$. The blue line represents the derived reduction potential for KC_{24} based on the charge utilisation yield during the reaction with $ZnCl_2$.

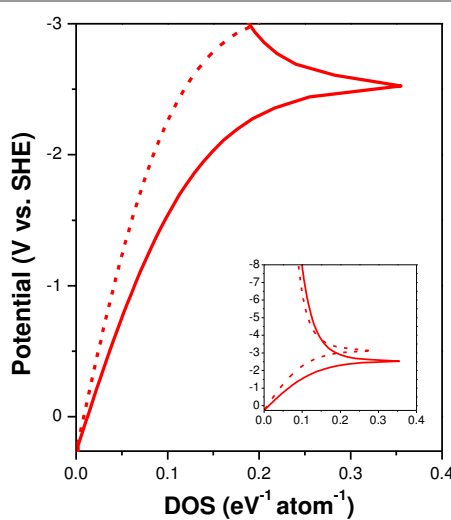


Fig. 6 Semi-quantitative estimate of Coulombic effects on the graphene DOS. The solid curve represents the tight-binding DOS as used above. The dashed and dotted curves represent the possible effect of Coulombic interactions due to the additional electron density in doped graphene. Inset shows the modified graphene DOS over a wider potential range.

Coulombic interactions that increase with added electron density are likely to affect the DOS such that there is a non-linear “stretching” of the density of states. This effect is semi-quantitatively represented in Fig. 6. Here, the potentials in the

DOS plot are shifted with the addition of successive electron density, by the equation⁴⁴ $\Delta V = ne/C$, where ne is the added electron density and C is the capacitance. Qualitatively, with increased Coulombic repulsion, a slightly more reducing KC_8 potential would be obtained relative to the potentials derived above. This effect may explain the shift in range between Figs. 5A and 5B, and in particular the deposition of manganese. In addition, the change in shape of the DOS would tend to bring the estimates based on the different metals closer together. However, further theoretical simulations that incorporate both Coulombic and solvation effects are required to complement the proposed theory.

Experimental

Nanocarbon polyelectrolyte preparation and subsequent reactions were performed by SAH inside a nitrogen-filled Lab Master SP glove box (mBraun, Germany) containing < 1 ppm O_2 , H_2O at all times unless stated.

Preparation of charged carbon polyelectrolytes

HiPco nanotubide salt (NaC_{10}) was produced by DJB using the sodium/liquid ammonia reduction method⁵ using raw HiPco

SWCNT powder (Batch: R2-172, NanoIntegris, USA). After removing the ammonia, the remaining nanotubide salt was added to DMF (anhydrous grade, 99.8% further dried by 3 Å molecular sieves, both purchased from Sigma-Aldrich, UK) and left to spontaneously dissolve for at least 7 days. Fractions of the supernatant were then taken for subsequent reactions.

KC₈ and KC₂₄ were made by CAH and PLC, respectively, using the vapour transport method from natural flake graphite (Madagascar)²⁰ and were confirmed to be phase pure by X-ray diffraction (within the limits of the measurement). For each experiment, 20 mL, NMP (anhydrous grade, 99.5%, further dried by 4 Å molecular sieves, both purchased from Sigma-Aldrich, UK), was added to 10 mg KC_x in a 100 mL Young's tap Schlenk tube. The sample was removed from the glove box, mildly sonicated for 30 min (ultrasonic cleaner, VWR, UK) and returned to the glove box for subsequent reactions.

Metal salts/complexes

MnCl₂ (anhydrous, beads, -10 mesh, 99.999% trace metals basis), ZnCl₂ (anhydrous, beads, amorphous, ~10 mesh, 99.99% trace metals basis) and CuCl₂ (99.999% trace metals basis) were purchased from Sigma-Aldrich, UK, and used as-received. CuMes was purchased from Strem Chemicals, UK, and used as-received.

Nanotubide polyelectrolyte reactions

MCl₂ salt (M = Mn, Zn) was added to 3 mL DMF and added to 2 mL nanotubide dispersion (~1.2 mg nanotubide). An overall stoichiometry of 3:1 M:Na was used. The reaction was left to stir for 24 h before being removed from the glove box, washed and filtered under vacuum with 100 mL each of DMF, water, chloroform and ethanol (reagent grade, from Sigma-Aldrich, UK, and VWR, UK). Products were characterised by TGA and SEM.

Graphenide polyelectrolyte reactions

0.1 M stock solutions of MX₂ (M = Mn, Zn and Cu) salts and CuMes were made in NMP. Aliquots were added to the KC_x dispersion to give the desired stoichiometry of metal to potassium. The reaction was left to stir for 72 h before being removed from the glove box, washed and filtered under vacuum with 100 mL each of NMP, water, chloroform and ethanol. Products were dried and characterised as detailed in main article. The KC₈-CuMes sample was precipitated with toluene and centrifuged before filtration of the sediment. Air-free centrifugation was performed using a Sigma 2-16K centrifuge with Sigma 12139-H rotor at 15,000 g, 30 min. FEP Oak Ridge centrifuge tubes (Thermo Scientific, UK) were used and sealed with PTFE tape to maintain an inert environment. The sediment was filtered under vacuum with 100 mL each of toluene, THF, NMP, water, chloroform and ethanol (reagent grade, from Sigma-Aldrich, UK, and VWR, UK).

Characterisation techniques

Scanning electron microscopy (SEM). SEM was carried out by DBA and HHT on a high resolution field emission gun scanning electron microscope (FEGSEM) Leo Gemini 1525, with a built-in energy dispersive and wavelength dispersive X-ray spectrometer (EDX) (INCA, using INCA suite software V4.15, 2009, Oxford Instruments Plc., UK). Images were taken with an aperture of 30 µm typically at 5 keV. The gun voltage was increased to 15 keV for EDX spectra.

SEM/EDX samples were prepared on Al stubs using either silver dag, Leit adhesive carbon tabs or solution drop cast onto Al foil covered stubs. All SEM preparation products purchased from Agar Scientific, UK with Al foil supplied by VWR, UK. A representative EDX blank spectra was taken at regions away from the observed nanoparticles to ensure spectra were representative.

Thermogravimetric analysis (TGA). TGA experiments were carried out by SAH. TGA for the analysis of nanotubide reactions was performed using a Perkin Elmer Pyris 1 TGA. Samples were heated from 30 to 100 °C at 10 °C/min, and then held isothermally at 100 °C for 30 min in an inert atmosphere (N₂, 60 mL/min) to remove residual solvents. The temperature was then ramped to 850 °C at 10 °C/min in an oxidative atmosphere (air, 60 mL/min).

TGA for the analysis of graphenide reactions was performed using a Mettler Toledo TGA/DSC 1 with a GC200 flow controller. The TGA was coupled to a mass spectrometer (Hiden MS fitted with a 200 a.u. quadrupole sensor). Samples were heated from 30 to 100 °C at 35 °C/min, and then held isothermally at 100 °C for 30 min in an inert atmosphere (N₂, 60 mL/min) to remove residual solvents. The temperature was then ramped to 850 °C at 10 °C/min with a switch from N₂ to air at 600 °C. An inert gas flow was used between 100-600 °C to ensure there was no weight loss from trapped solvents, that would change the overall calculated carbon mass.

Inductively coupled plasma atomic emission spectroscopy (ICP-AES). ICP-AES was performed by SAH using a Perkin Elmer ICP 2000 DV OES (dual view optical emission spectrometer) in axial mode. Data was recorded using WinLab32 software. TGA residues (0.1-0.3 mg) were dissolved in 10 mL 10% HCl in water and further diluted by a factor of 10 for sampling. Calibration was performed using 1, 5 and 25 ppm solutions of ICP multi-element standard solution IV (Merck, Germany). A blank 10% HCl in water sample was carried out immediately following calibration, as a reference point for samples.

X-ray photoelectron spectroscopy (XPS). XPS spectra of powdered graphite samples were recorded by RM using a Thermo Scientific K-Alpha instrument using focused (400 µm spot) monochromatic Al-Kα radiation at a pass energy of 40 eV. The binding energies were referenced to the sp² C 1s peak of graphite at 284 eV.

UV-vis absorption spectroscopy. UV-vis spectroscopy was performed by SAH using a Perkin Elmer Lambda 950

spectrometer with samples measured in a sealed 4 mm path length optical glass cuvette.

Electrochemical characterisation. A Solartron 1287 Potentiostat (Solartron Analytical, UK) was used for the cyclic voltammetric (CV) measurements using CorrWare 2 software. CV experiments were performed inside a glove box. Experiments and analysis were performed by SAH and HHT. A 10 mL three electrode electrochemical cell was used, with platinum wire working and counter electrodes (Laboratory Reagent, 0.5 x 100 mm) purchased from Fisher Scientific, UK. The reference electrode, Ag/Ag⁺, containing 0.01 M silver nitrate and 0.1 M tetrabutylammonium perchlorate in acetonitrile, was purchased from IJ Cambria Scientific, UK. Anhydrous (KClO₄) was purchased from Sigma-Aldrich and used as-received. Electrolytic solutions of 0.1 M KClO₄ in NMP were further dried by 3 Å molecular sieves and stored in a glove box.

Conclusions

In this paper, nanocarbon polyelectrolyte anions have been used to reduce a series of metal salts/complexes, to attempt to quantify the reduction potential of these charged solutions. In characterising the degree of functionalisation and charge utilisation yields, combined TGA and ICP-AES techniques have provided accurate quantification by overcoming issues arising from the presence of alkali metal hydr(oxides) in TGA residues and the surface sensitivity of techniques such as XPS. While it is difficult to confirm the exact electrochemical potentials of these dissolved, charged nanocarbons, the results obtained for potassium graphenide systems closely match previous experimental and theoretical predictions for partial and complete charge transfer from potassium to carbon. The reactivity is clearly dominated by the filling of the electronic DOS of these nanocarbons, benefitting from the solvation and subsequent dissociation of graphenide and K⁺ species. However, it is still not fully understood how the DOS may change as a function of doping, especially since electron affinities and Coulombic interactions will play a major role at increased charge densities. Particularly with carbon nanotubes, the distribution of charge will be determined by the specific nanotube physical properties (diameter, length), electronic type (metallic/semi-conducting), dielectric properties, and purity (metal catalyst / defective and amorphous carbons). The alkali metal type and its presence as the metallic form also have an important role. Other alkali metal GICs including LiC_x may demonstrate higher reactivity than KC₈, due to the higher reduction potential of Li and the ability to transfer more charge (LiC₆). However, solvation effects will play a key role in determining the GIC chemical activity.

To summarise, future experiments investigating a complete set of metal salts/complexes may allow the accurate determination of nanocarbon reduction potentials. Understanding these potentials, the nature of the electron transfer, and the extent of

remaining unused charge, will help to improve the functionalisation of these technological relevant advanced carbons. As an aside, the observed production of metal nanoparticles is an interesting phenomenon, and may be applicable for a whole range of materials, from catalysts to nanoelectronic devices. Further nanoparticle stability and microscopy studies are required to probe the possible size distribution control that can be achieved with different stoichiometry.

Acknowledgements

The authors would like to thank EPSRC EP/G007314/1 and EP/L001896/1 for funding. HHT would like to thank the National Research Foundation, Energy Innovations Programme Office, Singapore.

Notes and references

^aDepartment of Chemistry, Imperial College London, London, SW7 2AZ, UK

^bDepartment of Physics and Astronomy, University College London, London, WC1E 6BT, UK

* E-mail: m.shaffer@imperial.ac.uk

Electronic Supplementary Information (ESI) available: Further characterisation of nanocarbon reactions (TGA, ICP-AES, XPS, UV-vis). Electrochemical measurements of metal compounds including the derivation of their reduction potentials. See DOI: 10.1039/b000000x/

1. M. S. Dresselhaus, G. Dresselhaus and P. Avouris, Carbon nanotubes: Synthesis, structure, properties, and applications, Springer, New York, 2001.
2. V. C. Moore, M. S. Strano, E. H. Haroz, R. H. Hauge, R. E. Smalley, J. Schmidt and Y. Talmon, *Nano Lett.*, 2003, **3**, 1379-1382.
3. S. D. Bergin, Z. Sun, P. Streich, J. Hamilton and J. N. Coleman, *The Journal of Physical Chemistry C*, 2010, **114**, 231-237.
4. T.-J. Park, S. Banerjee, T. Hemraj-Benny and S. S. Wong, *J. Mater. Chem.*, 2006, **16**, 141-154.
5. S. Fogden, C. A. Howard, R. K. Heenan, N. T. Skipper and M. S. P. Shaffer, *ACS Nano*, 2011, **6**, 54-62.
6. E. M. Milner, N. T. Skipper, C. A. Howard, M. S. P. Shaffer, D. J. Buckley, K. A. Rahnejat, P. L. Cullen, R. K. Heenan, P. Lindner and R. Schweins, *J. Am. Chem. Soc.*, 2012, **134**, 8302-8305.
7. C. A. Howard, H. Thompson, J. C. Wasse and N. T. Skipper, *J. Am. Chem. Soc.*, 2004, **126**, 13228-13229.
8. C. A. Howard, J. C. Wasse, N. T. Skipper, H. Thompson and A. K. Soper, *The Journal of Physical Chemistry C*, 2007, **111**, 5640-5647.
9. A. Catheline, C. Valles, C. Drummond, L. Ortolani, V. Morandi, M. Marcaccio, M. Iurlo, F. Paolucci and A. Pénicaud, *Chem. Commun.*, 2011, **47**, 5470-5472.
10. A. Pénicaud, P. Poulin, A. Derré, E. Anglaret and P. Petit, *J. Am. Chem. Soc.*, 2005, **127**, 8-9.
11. S. A. Hodge, S. Fogden, C. A. Howard, N. T. Skipper and M. S. P. Shaffer, *ACS Nano*, 2013, **7**, 1769-1778.
12. S. A. Hodge, M. K. Bayazit, H. H. Tay and M. S. P. Shaffer, *Nat Commun*, 2013, **4**.

13. Y. Chen, R. C. Haddon, S. Fang, A. M. Rao, P. C. Eklund, W. H. Lee, E. C. Dickey, E. A. Grulke, J. C. Pendergrass, A. Chavan, B. E. Haley and R. E. Smalley, *J. Mater. Res.*, 1998, **13**, 2423-2431.
14. M. K. Bayazit, A. Suri and K. S. Coleman, *Carbon*, 2010, **48**, 3412-3419.
15. R. Graupner, J. Abraham, D. Wunderlich, A. Vencelová, P. Lauffer, J. Röhrl, M. Hundhausen, L. Ley and A. Hirsch, *J. Am. Chem. Soc.*, 2006, **128**, 6683-6689.
16. D. Wunderlich, F. Hauke and A. Hirsch, *Chemistry – A European Journal*, 2008, **14**, 1607-1614.
17. A. Mukherjee, R. Combs, J. Chattopadhyay, D. W. Abmayr, P. S. Engel and W. E. Billups, *Chem. Mater.*, 2008, **20**, 7339-7343.
18. J. Chattopadhyay, S. Chakraborty, A. Mukherjee, R. Wang, P. S. Engel and W. E. Billups, *The Journal of Physical Chemistry C*, 2007, **111**, 17928-17932.
19. F. Hof, S. Bosch, S. Eigler, F. Hauke and A. Hirsch, *J. Am. Chem. Soc.*, 2013, **135**, 18385-18395.
20. C. A. Howard, M. P. M. Dean and F. Withers, *Phys. Rev. B*, 2011, **84**, 241404.
21. S. A. Hodge, M. K. Bayazit, K. S. Coleman and M. S. P. Shaffer, *Chem. Soc. Rev.*, 2012, **41**, 4409-4429.
22. Y. Tanaka, Y. Hirana, Y. Niidome, K. Kato, S. Saito and N. Nakashima, *Angew. Chem.*, 2009, **48**, 7655-7659.
23. Y. Hirana, Y. Tanaka, Y. Niidome and N. Nakashima, *J. Am. Chem. Soc.*, 2010, **132**, 13072-13077.
24. D. Paolucci, M. M. Franco, M. Iurlo, M. Marcaccio, M. Prato, F. Zerbetto, A. Pénicaud and F. Paolucci, *J. Am. Chem. Soc.*, 2008, **130**, 7393-7399.
25. H. C. Choi, M. Shim, S. Bangsaruntip and H. Dai, *J. Am. Chem. Soc.*, 2002, **124**, 9058-9059.
26. M. K. Bayazit, S. A. Hodge, A. R. J. Clancy, R. Menzel, S. Chen and M. S. P. Shaffer, unpublished work.
27. A. R. J. Clancy, M. K. Bayazit, S. A. Hodge and M. S. P. Shaffer, unpublished work.
28. J. F. Bondi, K. D. Oyler, X. Ke, P. Schiffer and R. E. Schaak, *J. Am. Chem. Soc.*, 2009, **131**, 9144-9145.
29. S. R. Ghanta, M. H. Rao and K. Muralidharan, *Dalton Transactions*, 2013, **42**, 8420-8425.
30. P. Hadley, Density of states of a graphene crystal in the tight-binding approximation, http://lamp.tugraz.ac.at/~hadley/ss1/bands/tbtable/2d_graphene_dos.html.
31. M. S. Dresselhaus and G. Dresselhaus, *Advances in Physics*, 1981, **30**, 139-326.
32. D. Savoia, C. Trombini and A. Umanironchi, *Pure Appl. Chem.*, 1985, **57**, 1887-1896.
33. A. Weitz and M. Rabinovitz, *Synth. Met.*, 1995, **74**, 201-205.
34. L. B. Ebert, D. R. Mills and J. C. Scanlon, *Mater. Res. Bull.*, 1982, **17**, 1319-1328.
35. L. B. Ebert, *Carbon*, 1985, **23**, 585-587.
36. Z.-H. Pan, J. Camacho, M. H. Upton, A. V. Fedorov, C. A. Howard, M. Ellerby and T. Valla, *Phys. Rev. Lett.*, 2011, **106**, 4.
37. S. A. Solin and H. Zabel, *Advances in Physics*, 1988, **37**, 87-254.
38. D. Voiry, C. Drummond and A. Penicaud, *Soft Matter*, 2011, **7**, 7998-8001.
39. S. Pisana, M. Lazzeri, C. Casiraghi, K. S. Novoselov, A. K. Geim, A. C. Ferrari and F. Mauri, *Nat Mater.*, 2007, **6**, 198-201.
40. M. Takahashi, J. Kamada, K. Iwata, K. Goto, H. Watanabe and S. Tamai, *Bull. Chem. Soc. Jpn.*, 2008, **81**, 168-170.
41. C. Barriere, K. Piettre, V. Latour, O. Margeat, C.-O. Turrin, B. Chaudret and P. Fau, *J. Mater. Chem.*, 2012, **22**, 2279-2285.
42. M. Singh, I. Sinha, M. Premkumar, A. K. Singh and R. K. Mandal, *Colloids and Surfaces A: Physicochemical and Engineering Aspects*, 2010, **359**, 88-94.
43. N. T. Mai, T. T. Thuy, D. M. Mott and S. Maenosono, *CrystEngComm*, 2013, **15**, 6606-6610.
44. R. W. Murray, *Chem. Rev.*, 2008, **108**, 2688-2720.